



HAL
open science

Shigella promotes major alteration of gut epithelial physiology and tissue invasion by shutting off host intracellular transport

Mariana Ferrari, Valérie Malardé, Laura Salavessa, Giulia Nigro, Stéphane Descorps-Declère, John Rohde, Pamela Schnupf, Vanessa Masson, Guillaume Arras, Damarys Loew, et al.

► To cite this version:

Mariana Ferrari, Valérie Malardé, Laura Salavessa, Giulia Nigro, Stéphane Descorps-Declère, et al.. Shigella promotes major alteration of gut epithelial physiology and tissue invasion by shutting off host intracellular transport. Proceedings of the National Academy of Sciences of the United States of America, 2019, 10.1073/pnas.1902922116 . pasteur-02167942

HAL Id: pasteur-02167942

<https://pasteur.hal.science/pasteur-02167942>

Submitted on 3 Jun 2020

HAL is a multi-disciplinary open access archive for the deposit and dissemination of scientific research documents, whether they are published or not. The documents may come from teaching and research institutions in France or abroad, or from public or private research centers.

L'archive ouverte pluridisciplinaire **HAL**, est destinée au dépôt et à la diffusion de documents scientifiques de niveau recherche, publiés ou non, émanant des établissements d'enseignement et de recherche français ou étrangers, des laboratoires publics ou privés.

Shigella promotes major alteration of gut epithelial physiology and tissue invasion by shutting off host intracellular transport

Mariana L. Ferrari^{1,2}, Valérie Malardé^{1,2}, Alexandre Grassart^{1,2}, Laura Salavessa^{1,2,3}, Giulia Nigro^{1,2}, Stéphane Decorps-Declere⁴, John R. Rohde⁵, Pamela Schnupf⁶, Vanessa Masson⁷, Guillaume Arras⁷, Damarys Loew⁷, Philippe J. Sansonetti^{1,2,8*}, Nathalie Sauvonnet^{1,2*}

¹ Unité de Pathogénie Microbienne Moléculaire, Institut Pasteur, 28 rue du Dr Roux, 75015, Paris, France ² U1202, INSERM, Paris, France ³ Université Paris Sud, Paris-Saclay University, Orsay, France ⁴ Institut Pasteur – Hub Bioinformatique et Biostatistique – C3BI, USR 3756 IP CNRS – 28 rue du Dr Roux, 75015, Paris, France ⁵ Department of Microbiology and Immunology, Dalhousie University, Halifax, NS, Canada ⁶ Institut Necker Enfants Malades, INSERM-CNRS, Laboratory of Host-Microbiota Interaction, 156 rue de Vaugirard, 75015 Paris, France ⁷ Institut Curie, PSL Research University, Centre de Recherche, Laboratoire de Spectrométrie de Masse Protéomique, 26 rue d'Ulm, Paris 75248 Cedex 05, France ⁸ Chaire de Microbiologie et Maladies Infectieuses, Collège de France, Paris, France

Submitted to Proceedings of the National Academy of Sciences of the United States of America

Intracellular trafficking pathways in eukaryotic cells are essential to maintain organelle identity and structure, and to regulate cell communication with its environment. *Shigella flexneri* invades and subverts the human colonic epithelium by the injection of virulence factors through a type 3 secretion system (T3SS). In this work we report the multiple effects of two *S. flexneri* effectors, IpaJ and VirA, which target small GTPases of the Arf and Rab families, consequently inhibiting several intracellular trafficking pathways. IpaJ and VirA induce large-scale impairment of host protein secretion and block the recycling of surface receptors. Moreover, these two effectors decrease clathrin-dependent and -independent endocytosis. Therefore, *S. flexneri* infection induces a global blockage of host cell intracellular transport, affecting the exchange between cells and their external environment. The combined action of these effectors disorganizes the epithelial cell polarity, disturbs epithelial barrier integrity, promotes multiple invasion events and enhances the pathogen capacity to penetrate into the colonic tissue *in vivo*.

bacteria | pathogen | secretion | endocytosis | polarity

Introduction

Eukaryotic cells contain a complex array of intracellular membrane-bound compartments, which mediate cell communication with their environment by the bi-directional transport of proteins and lipids between the intracellular and extracellular spaces. This occurs via two main mechanisms: the secretory and the endocytic trafficking pathways. The efficient intracellular transport of molecules is regulated by GTPases of the Arf, Rab, Rho and dynamin families and is critical to maintain organelle identity and structure. Additionally, the coordination of intracellular trafficking with other pathways regulates vital processes including cell polarity, immunity, signaling and development as well as tissue and organ functions (1–3).

Shigella spp are Gram-negative intracellular bacteria causing bacillary dysentery or shigellosis (4). *Shigella* invades the colonic epithelium by using a type 3 secretion system (T3SS) that enables the injection of more than 20 virulence factors, the so-called effectors, into the cell (5, 6). These effectors then target multiple cellular functions to promote non-phagocytic uptake, followed by intracellular bacterial replication, cell-to-cell spreading, and subsequently leading to destruction of the colonic epithelium (7, 8). While the enzymatic functions for most effectors has been described and analyzed in cell culture, the mechanisms by which they cooperate with one another to promote infection remains largely unknown. *S. flexneri* induces Golgi apparatus fragmentation and reorganization of the endocytic compartment, leading to a block in secretion and receptor recycling (9). Among the

arsenal of injected effectors, two have been specifically implicated in targeting host cell small GTPases essential for Golgi-mediated secretory transport, namely: IpaJ and VirA. IpaJ is a cysteine protease catalyzing the cleavage of myristoylated glycine residues primarily from ADP-ribosylation factor (Arf) and Arf-like (Arl) proteins (10, 11). As a consequence, it was shown that IpaJ inhibits STING-mediated activation of the interferon (IFN) pathway by blocking STING translocation from the endoplasmic reticulum (ER) to ER-Golgi intermediate compartment (ERGIC) (12). Conversely, VirA was reported to impair host cell secretory transport, in addition to inhibiting autophagy (13, 14), by acting as a Rab-GTP activating protein (GAP) with preferential targeting of Rab1, as shown *in vitro* (13). Although the catalytic activities of these two effectors have been well described, it remains to be elucidated if both act in synergy or independently, and which changes they induce in the intestinal tissue during *S. flexneri* infection.

In eukaryotes, Arf and Rab protein families work together to regulate intracellular trafficking pathways. However, the exact mechanisms of coordination of action are not yet fully understood. Given that these small GTPases are targeted by both IpaJ

Significance

***Shigella flexneri* is an enteroinvasive prokaryote that induces human bacillary dysentery. The delivery of around 30 bacterial effectors inside colonic epithelial cells allows the pathogen to invade, replicate and move into adjacent cells, hence subverting cellular and immune functions of its host. Intracellular trafficking pathways in eukaryotic cells are essential to regulate cell communication with their environment. Our work shows that two effectors of *Shigella flexneri* block three main trafficking pathways of its host cell: secretion, recycling and endocytosis, thereby freezing the exchange through the plasma membrane. As a consequence, *Shigella flexneri* disorganizes the epithelial cell polarity, disturbs epithelial barrier integrity, and enhances the pathogen capacity to penetrate into the colonic tissue *in vivo*.**

Reserved for Publication Footnotes

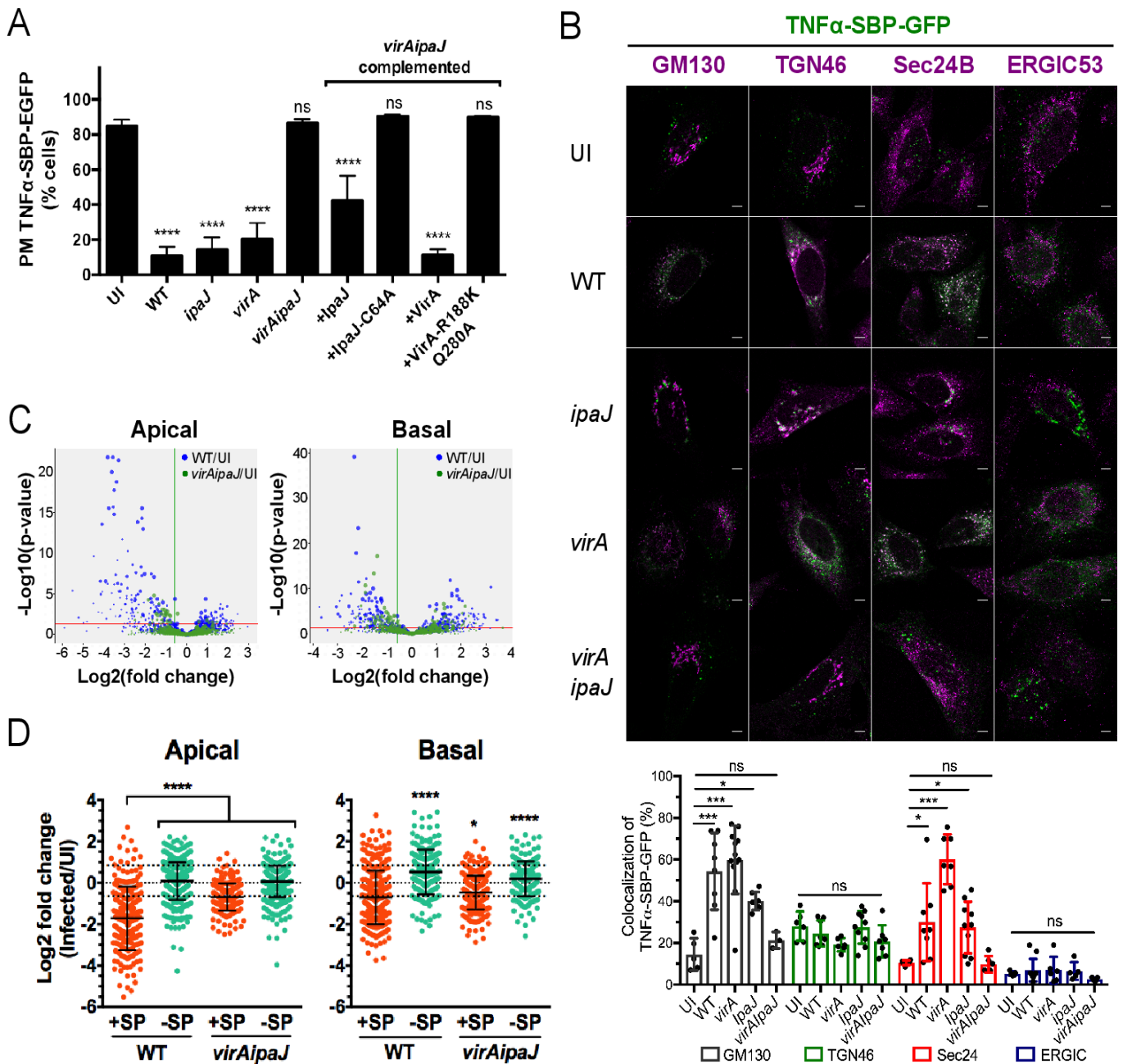


Fig. 1. *S. flexneri* effectors IpaJ and VirA have a global effect on conventional secretion. (A) IpaJ and VirA effectors block the anterograde transport of the cytokine TNF α . HeLa cells stably expressing the RUSH cargo TNF α -SBP-GFP and the molecular hook Streptavidin-KDEL were uninfected (UI) or infected for 1 hour with WT-dsRed or the dsRed-expressing mutants *ipaJ*, *virA*, *virAipaJ*, or with *virAipaJ* complemented with plpaJ-myc, plpaJ-C64-myc, pVirA-myc, or pVirA-R188K/Q280A-myc. Cells were then incubated with biotin for 1 hour, fixed and surface-stained for TNF α -SBP-GFP with anti-GFP DyLight 680 conjugated antibody. The arrival of TNF α -SBP-GFP to the plasma membrane (PM) was monitored by flow cytometry. Mean SD. n = 3. ****p<0.0001, ns: non-significant (one-way ANOVA, Dunnett's *post-hoc* test, compared to UI). (B) TNF α -SBP-GFP is retained in different subcellular compartments upon *S. flexneri* infection. HeLa cells stably expressing the RUSH cargo TNF α -SBP-GFP and the molecular hook Streptavidin-KDEL were uninfected (UI) or infected for 1 hour and incubated with biotin for 1 additional hour. Cells were fixed, permeabilized and stained with various subcellular markers: anti-GM130 (*cis*-Golgi), anti-ERGIC53 (ERGIC), anti-Sec24B (ERES), anti-TGN46 (*trans*-Golgi network). Scale bar: 5 μ m. Levels of colocalization between TNF α -SBP-GFP and the different sub-cellular markers were quantified by SODA plugin in ICY software. Mean SD, 5<n<12 cells. *p<0.05; ***p<0.001 (one-way ANOVA, Dunnett's *post-hoc* test). (C-D) *S. flexneri* blocks globally the host conventional secretion. Caco-2/TC7 cells were labeled with SILAC amino acids, grown in transwell filters and infected with WT *S. flexneri* or the mutant *virAipaJ*. After 4.5 hours, the apical and basal media were collected and analyzed by mass spectrometry to determine the relative abundance of secreted proteins in the infected, in comparison with UI conditions. (C) Volcano plots displaying log2 fold-changes of secreted proteins from WT or *virAipaJ* infected cells in comparison with UI conditions in apical and basal media. (D) Dot plots represent log2 of infected/UI ratio for proteins with (red) and without (green) signal peptide (SP). Mean SD. 217>n>394 proteins for Apical secretome; 194>n>281 proteins for Basal secretome. *p<0.05, ****p<0.0001 (one-way ANOVA, Dunnett's *post-hoc* test, each condition compared to Apical or Basal secreted proteins containing signal peptide (+SP)).

and VirA, it raises the question if these effectors further affect

other trafficking pathways in addition to the known secretory transport.

273
274
275
276
277
278
279
280
281
282
283
284
285
286
287
288
289
290
291
292
293
294
295
296
297
298
299
300
301
302
303
304
305
306
307
308
309
310
311
312
313
314
315
316
317
318
319
320
321
322
323
324
325
326
327
328
329
330
331
332
333
334
335
336
337
338
339
340

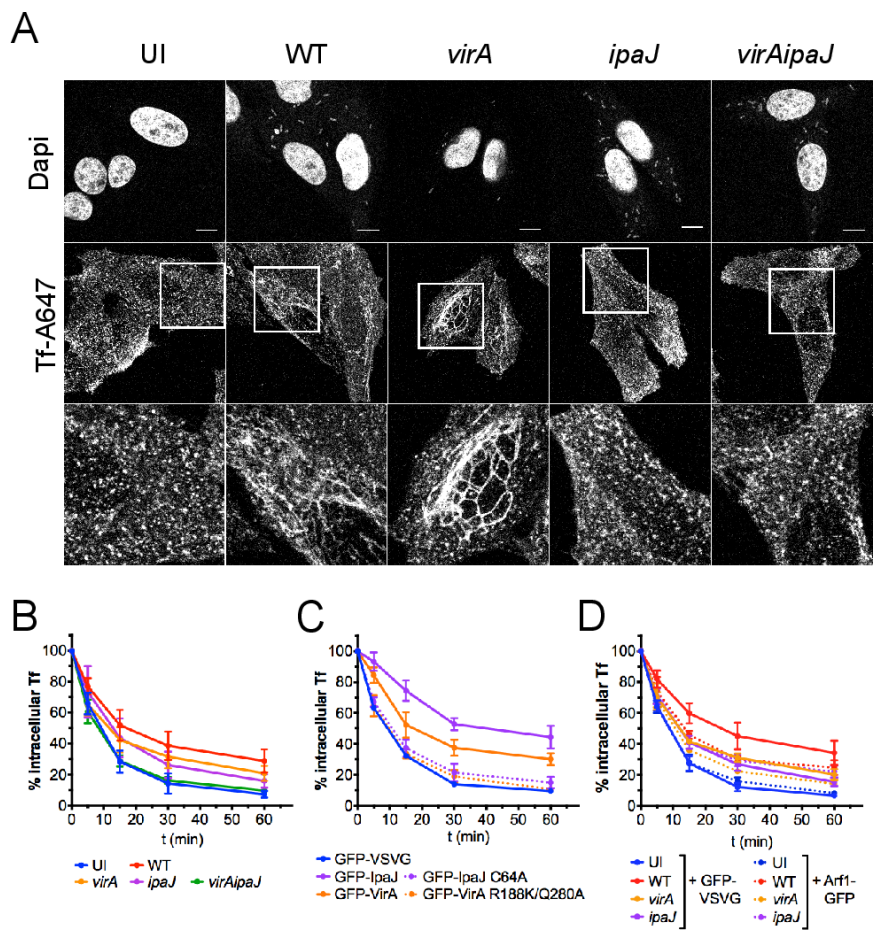


Fig. 2. Both *S. flexneri* IpaJ and VirA affect TfR recycling. (A) IpaJ induces endosomal tubulation. Hep2 cells loaded with Tf-AF647 were uninfected (UI) or infected for 1 hour with WT, *virA*, *ipaJ* or *virAipaJ* strains, fixed and stained with Dapi (nuclei and bacteria). Scale bar: 10 μ m. (B-D) Tf recycling kinetics monitored by FC. Hep2 cells non-transfected or transfected with the indicated plasmids were loaded with Tf-AF647 and were left UI or infected for 1 hour with the indicated *S. flexneri* strains. Cells were then chased with unlabeled holo-Tf, and the loss of intracellular Tf-AF647 fluorescence was monitored over time. (B) IpaJ and VirA block Tf recycling. Cells were UI or infected with WT, *virA*, *ipaJ* or *virAipaJ* strains followed by Tf recycling kinetic. (C) Tf recycling is inhibited by IpaJ and VirA catalytic activities. Cells were transfected with GFP-VSVG (control), GFP-VirA, GFP-IpaJ or their mutated versions GFP-VirA-R188K/Q280A and GFP-IpaJ-C64A. Tf recycling kinetic was performed 24 hours post-transfection. (D) Arf1-GFP overexpression partially recovers Tf recycling. Cells were transfected either with GFP-VSVG (control) or Arf1-GFP, loaded with Tf-AF647, UI or infected with WT, *virA* or *ipaJ* strains followed by Tf recycling. Means SD from at least 3 independent experiments are shown (statistical tests in Fig. S2D-F).

Here, we demonstrate that these two effectors independently block global host cell secretion and concurrently operate to impair receptor recycling. Moreover, we report that IpaJ and VirA decrease receptor-mediated endocytosis. Our results illustrate how *S. flexneri* “freezes” the invaded host cell by globally interfering on multiple intracellular transport systems, thereby affecting the exchange of molecules between cells and their environment and consequently cell and tissue functions.

Results

***S. flexneri* effectors IpaJ and VirA globally impair conventional secretion**

Both IpaJ and VirA *S. flexneri* effectors have been shown to affect Golgi-mediated transport in host cells (10, 13), raising the question as to whether these effectors operate in synergy or independently. To address this, we first quantified the secretion level of the cytokine TNF α upon infection with wild type (WT) *S. flexneri*, or the mutant strains *ipaJ*, *virA*, or *virAipaJ*. We used the RUSH system (15) to follow the synchronized trafficking of the reporter TNF α -SBP-GFP from the endoplasmic reticulum to the plasma membrane of epithelial cells (Fig. 1A). Infection with WT *S. flexneri* blocked 75% of the anterograde trafficking of TNF α -SBP-GFP when compared to uninfected cells (UI), in line with previous reports on other cargoes (9, 13). Similar results were obtained when cells were infected with either *ipaJ* or *virA* *S. flexneri* single mutants. However, in cells infected by the *virAipaJ* double mutant, TNF α -SBP-GFP transport levels were similar to the uninfected condition (Fig. 1A). This differential effect of trafficking during infection by WT, *ipaJ*, *virA* and *virAipaJ* was not due to impairment in bacterial invasion by the mutant strains (Fig.

S1A). Complementation of the double mutant with either pVirA-myc or pIpaJ-myc was sufficient to restore, at least partially, the secretion inhibitory phenotype obtained with WT bacteria. As expected, complementation with the mutated versions of these effectors in their catalytic sites, pVirA-R188K/Q280A-myc or pIpaJ-C64A-myc (10, 13), did not affect the normal trafficking of TNF α -SBP-GFP (Fig. 1A). Altogether, these results show that each effector, IpaJ and VirA, is sufficient to block anterograde transport of the cargo via their catalytic activities and hence acts largely independently.

To determine in which subcellular compartment TNF α -SBP-GFP was retained upon *S. flexneri* infection, we utilized immunostaining of various subcellular compartments after 1 hour of synchronized trafficking and quantified the percentage of colocalization using a statistical object-based method (Fig. 1B). In uninfected and *virAipaJ* infected cells, TNF α -SBP-GFP was mostly at plasma membrane (Fig. 1A), but the minor intracellular pool was mostly colocalized with *trans*-Golgi network (TGN) labeled with TGN46 (21-28%) and with *cis*-Golgi remnants (GM130-positive compartment, 14-20%) (Fig. 1B). By contrast, in WT-infected cells TNF α -SBP-GFP was mostly intracellular (Fig. 1A) and colocalized with GM130 (54%), Sec24B (29%), a marker of ER exit sites (ERES), and with TGN46 (24%). This reveals that *S. flexneri* WT infection blocked the Golgi-mediated transport at different stages, mainly at ERES and at *cis*-Golgi. Interestingly, infection with *virA* or *ipaJ* mutants resulted in a phenotype similar to the WT strain except that in absence of IpaJ, TNF α -SBP-GFP was strongly colocalized with Sec24 (60%, Fig. 1B). These data suggest that the retention in the Sec24B-positive compartment was due to the action of IpaJ. We could not observe colocalization

341
342
343
344
345
346
347
348
349
350
351
352
353
354
355
356
357
358
359
360
361
362
363
364
365
366
367
368
369
370
371
372
373
374
375
376
377
378
379
380
381
382
383
384
385
386
387
388
389
390
391
392
393
394
395
396
397
398
399
400
401
402
403
404
405
406
407
408

409
410
411
412
413
414
415
416
417
418
419
420
421
422
423
424
425
426
427
428
429
430
431
432
433
434
435
436
437
438
439
440
441
442
443
444
445
446
447
448
449
450
451
452
453
454
455
456
457
458
459
460
461
462
463
464
465
466
467
468
469
470
471
472
473
474
475
476

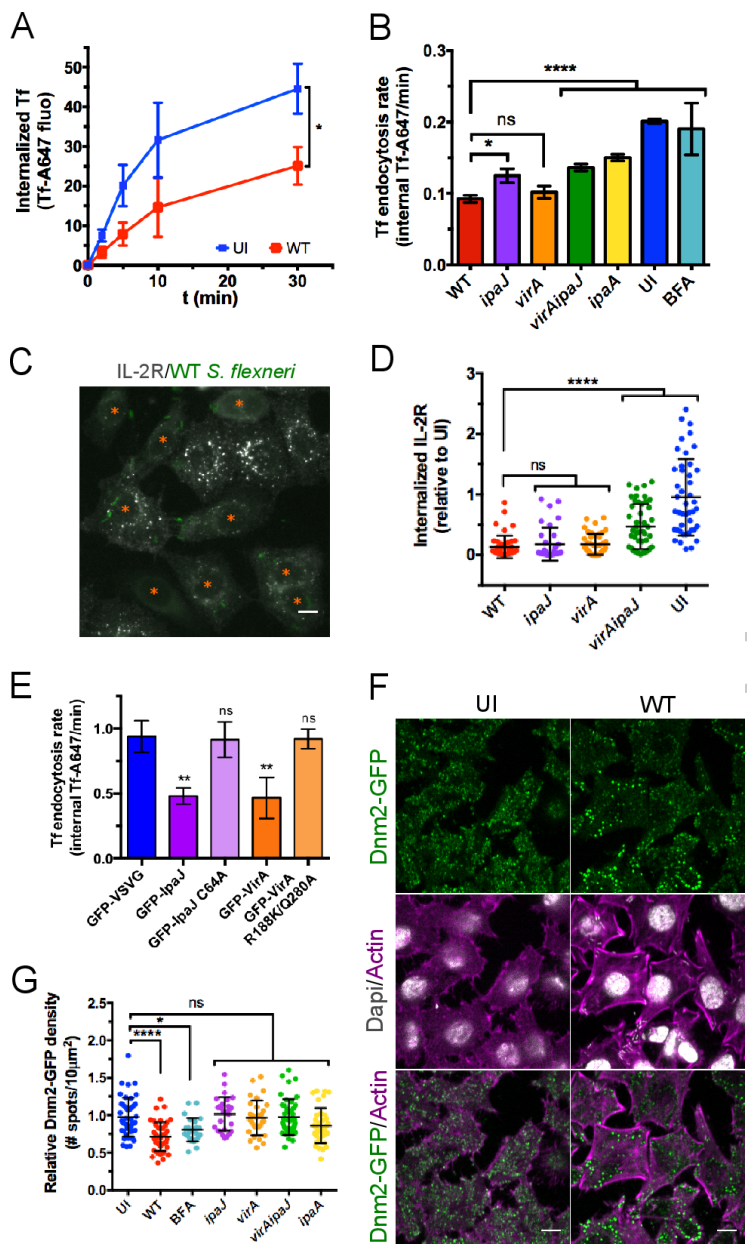


Fig. 3. *S. flexneri* affects clathrin-dependent and independent endocytosis. (A) Tf uptake is decreased upon WT-infection. Hep2 cells were left uninfected (UI) or infected with the WT strain for 30 min and then incubated for different time-points with Tf-AF647 at 37 °C. After an acidic wash, the total internal Tf-AF647 fluorescence was quantified by FC. Mean SD, n = 4. *p<0.05 (unpaired two-tailed Welch's t-test performed on AUC). (B) Different *S. flexneri* effectors decrease the Tf endocytosis rate. Hep2 cells were left UI or infected with GFP-expressing WT or mutant strains for 90 min, prior to monitor by FC the Tf-AF647 uptake over time. Mean SD. n 3. (C-D) IL-2R endocytosis is decreased upon WT *S. flexneri* infection. (C) UI or WT-infected Hep2β cells were incubated with an anti-IL-2Rβ-Cy3 antibody for 15 min at 37°C, fixed and subjected to fluorescent microscopy. Scale bar: 10 μm. (D) Quantification of IL-2R endocytosis. Cells either UI or infected by WT, *ipaJ*, *virA* and *virAipaJ* *S. flexneri* strains for 90 min were incubated with an anti-IL-2Rβ-Cy3 antibody for 30 min at 37°C, fixed, subjected to confocal fluorescence microscopy and analyzed by quantifying the fluorescence intensity of IL-2R-positive vesicles per cell. Mean SD. 35<n<48 cells. (E) Tf endocytosis kinetic was performed 24 hours post-transfection. Mean SD. n = 3. (F-G) *S. flexneri* decrease Dnm2-GFP density at plasma membrane. Hep2β Dnm2-GFP cells were UI, treated with BFA for 30 min or infected with WT or mutant strains for 90 min. Cells were fixed and labeled with rabbit anti-LPS followed by anti-rabbit-A405 and Phalloidin-A647 prior to confocal (F) or TIRF (G) imaging. Scale bar: 10 μm. (G) Quantification of Dnm2-GFP density (number of Dnm2-GFP spots/area) at plasma membrane from TIRF microscopy images. Mean SD. 27<n<45 cells pooled from 2 independent experiments. B-D-E-G, one-way ANOVA, Dunnett's *post-hoc* test. ns: non significant; *p<0.05; **p<0.01; ****p<0.0001.

of TNFα-SBP-GFP with ERGIC53, a marker of the ERGIC, in any of the conditions tested (Fig. 1B). Taken together, our data show that IpaJ and VirA block the anterograde trafficking at multiple stages, confirming their independent action in blocking host cell secretion.

To investigate the global effects of *S. flexneri* infection on the secretory transport in a polarized cell system, we used the SILAC technology coupled to LC-MS/MS (16). Polarized Caco-2/TC7 cells labeled with “medium” amino acids were uninfected, and cells labeled with “heavy” amino acids were infected with either WT *S. flexneri* or the mutant *virAipaJ*. After 5 hours of infection, the SILAC-labeled secretome-containing supernatants from the apical and basal side were collected and treated for mass spectrometry analysis in order to determine the relative abundance of peptides between infected and uninfected samples (Fig. S1B). Fold change-based GO enrichment analysis showed that apical and basal secretome proteins were more than 4-times enriched in extracellular proteins in comparison to the human

theoretical proteome, hence revealing the good quality of our analysis. We quantified 148 proteins in the apical and 136 in the basal supernatants that were differentially secreted in WT *S. flexneri* infected cells when compared to uninfected cells (UI), from which 125 (84%) and 79 (58%) proteins, respectively, were less secreted (Fig. 1C, Table S1). This secretion impairment was independent of global changes in the proteome of infected cells (Fig. S1C). In addition, tight junctions and cell viability were not affected during the secretome collection (Fig. S1D-F). Among the differentially secreted proteins, 116 (92.8%) of the apical and 64 (81%) of the basal proteins contained predicted cleavable signal peptides indicating targets of the conventional secretory pathway (Fig. 1D). In contrast, analysis of the same proteins from the *virAipaJ*-infected samples revealed only a marginal impairment on the secretion of signal-peptide containing proteins; indeed, the mean fold-change was less striking than for the WT-infected secretomes (Fig. 1D, Table S1). Taken together, these results indicate that *S. flexneri* infection affects the conventional

477
478
479
480
481
482
483
484
485
486
487
488
489
490
491
492
493
494
495
496
497
498
499
500
501
502
503
504
505
506
507
508
509
510
511
512
513
514
515
516
517
518
519
520
521
522
523
524
525
526
527
528
529
530
531
532
533
534
535
536
537
538
539
540
541
542
543
544

545
546
547
548
549
550
551
552
553
554
555
556
557
558
559
560
561
562
563
564
565
566
567
568
569
570
571
572
573
574
575
576
577
578
579
580
581
582
583
584
585
586
587
588
589
590
591
592
593
594
595
596
597
598
599
600
601
602
603
604
605
606
607
608
609
610
611
612

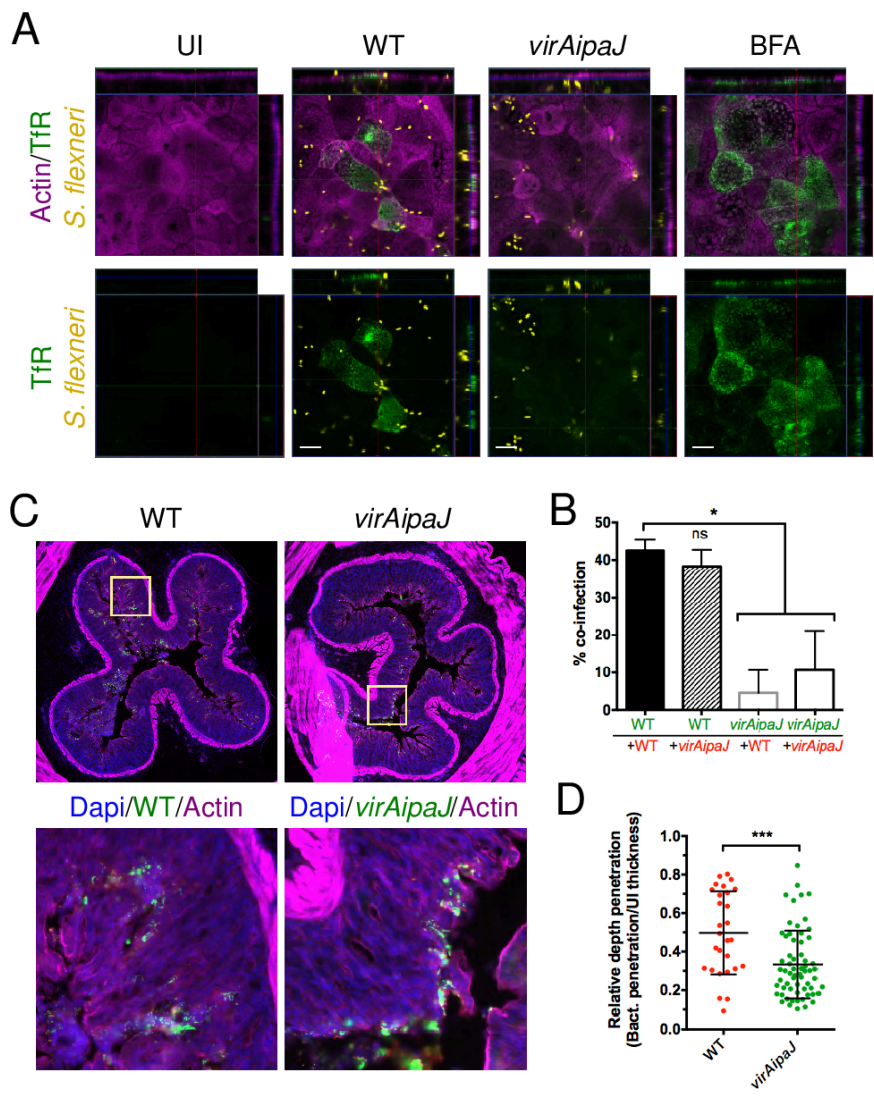


Fig. 4. *S. flexneri* invasion disrupts cell polarity and colonic epithelium(A) *S. flexneri* delocalizes the Tfr to the apical domain of polarized Caco-2/TC7 cells. Cells were left uninfected (UI), infected with the WT or *virAipaJ* strains for 5h or treated with BFA for 30 min, prior to fixation without permeabilization and subsequent apical surface staining with an anti-Tfr (OKT9) recognizing the extracellular domain of the receptor. Scale bars: 10 μ m. (B) IpaJ and VirA enhance re-infection of polarized cells. Caco-2/TC7 cells were primo-infected with GFP-expressing WT or *virAipaJ* strains (green) for 4 hours, and then re-infected with the same strains expressing dsRed for 2 more hours (red). The % of co-infection was quantified by determining the % of primo-infected cells (GFP positive) that were re-infected with dsRed-expressing bacteria. Mean SD, n = 4. ns: non significant; * p<0.05 (Kruskal-Wallis test followed by Dunn's *post-hoc* test). (C-D) *S. flexneri* WT has a deeper penetration than *virAipaJ* mutant into the Guinea pig colonic tissue. (C) Colonic tissue from animals infected with GFP-expressing WT or *virAipaJ* mutant, 8 hours post-infection, were stained with Phalloidin-A647 (actin) and Dapi (nuclei). (D) The relative depth penetration of both strains into the colonic tissue was measured by their penetration from the epithelial surface compared to the total epithelial mucosa thickness at 4 hours post-infection. Mean SD. 28<n<48 focus of infection pooled from 2 biological replicates. ***p<0.001 (Mann-Whitney test).

secretory pathway in a global manner, and that this is mediated by the action of both IpaJ and VirA effectors.

Among the proteins less secreted by WT-infected cells, the most represented class were hydrolytic enzymes, like proteases (cathepsin D, carboxypeptidase M) and enzyme regulators. However, we also found cell receptors (LDLR, HGFR), lipid transporters (apolipoproteins), proteins related to cell adhesion and extracellular matrix (ECM) (laminins), and immunomodulators (IL6ST) (Table S1). The secretion inhibition of this wide array of proteins may have severe consequences on cell polarity and intestinal tissue organization and functions.

***S. flexneri* effectors IpaJ and VirA both block the host cell recycling pathway**

As IpaJ and VirA effectors are targeting small GTPases from the Arf and Rab families, which are important for normal endosomal functioning (1, 3), we further investigated if they were also implicated in the previously described reorganization of the endosomal compartment and impairment of transferrin (Tf) receptor (TfR) recycling (9). We loaded Hep2 cells with fluorescent Tf coupled to Alexa Fluor 647 (Tf-AF647), prior to infection with WT, *virA*, *ipaJ* or *virAipaJ* strains (Fig. 2A). In line with what was previously reported (9), after 1 hour of infection with WT *S. flexneri* we observed an extensive formation of membrane tubules labeled with Tf-AF647, which resembled

the phenotype induced by the drug brefeldin A (BFA) (Fig. S2A) (17). A comparable, tubular phenotype was observed when cells were infected with the *virA* mutant strain. In contrast, in cells infected with either the *ipaJ* or *virAipaJ* mutant, Tf-AF647 was located in punctate vesicles throughout the cytoplasm, resembling the uninfected control (Fig. 2A). These findings demonstrate that IpaJ is involved in endosomal compartment tubulation. As shown in the case of BFA-treated cells (17, 18) (Fig. S2B), the formation of endosomal tubules is not necessarily linked to a striking recycling impairment. We therefore assessed TfR recycling kinetics by pulse-chase experiments. Here, cells were loaded with Tf-AF647, uninfected or infected for 1 hour with the GFP-expressing WT or mutant *S. flexneri* strains, and then chased with the unlabeled holo-Tf for different time-points prior to analysis by flow cytometry (FC) (Figs. 2B, S2D). We observed a notable reduction of Tf-AF647 recycling in WT-infected cells, whereby 50% of the internalized Tf-AF647 recycled back to the plasma membrane in 17 minutes, as compared to only 9 minutes for uninfected cells. In addition to the observed time delay induced by the WT strain, Tf recycling was also blocked, as indicated by 29% retention of Tf-AF647 at the 60 minutes kinetic end-point. When cells were infected with the *ipaJ* or *virA* mutant, an intermediate phenotype was observed while the *virAipaJ* double mutant had normal levels of Tf recycling similarly to uninfected conditions (Figs. 2B, S2D).

613
614
615
616
617
618
619
620
621
622
623
624
625
626
627
628
629
630
631
632
633
634
635
636
637
638
639
640
641
642
643
644
645
646
647
648
649
650
651
652
653
654
655
656
657
658
659
660
661
662
663
664
665
666
667
668
669
670
671
672
673
674
675
676
677
678
679
680

681 These results demonstrate that a combined action of these two
682 effectors is required to efficiently block receptor recycling in the
683 host cell. Further, we confirmed that the inhibitory effect of IpaJ
684 and VirA on receptor recycling is due to their catalytic activities.
685 While their ectopic expression in Hep2 cells dramatically de-
686 creased the Tf recycling rate (Figs. 2C, S2E), control levels of Tf
687 recycling were obtained when the VirA-R188K/Q280A or IpaJ-
688 C64A mutated versions were expressed (Figs. 2C, S2E). To gain
689 further insights into the mechanisms at play, we overexpressed
690 one of the targets of IpaJ, the small GTPase Arf1 fused to GFP,
691 prior to infection with dsRed-expressing bacterial strains (Figs.
692 2D, S2F). In uninfected cells the Tf recycling rate remained
693 unchanged despite overexpression of either Arf1-GFP or GFP-
694 VSFG, which served as a transfection control (Figs. 2D, S2C-F).
695 Interestingly, the rate of Tf recycling was faster in cells infected
696 by the IpaJ-expressing strains, WT and *virA*, and overexpressing
697 Arf1-GFP (Figs. 2D, S2F). In contrast, in *ipaJ*-infected cells, the
698 recycling kinetics remained unchanged by Arf1 overexpression.
699 These results strongly suggest that IpaJ slows down Tf recycling
700 by targeting Arf1. Overall, we demonstrate that the two *S. flexneri*
701 effectors, IpaJ and VirA, present catalytic activities that together
702 strongly inhibit two major trafficking pathways, secretion and
703 recycling, that are implicated in the delivery of molecules to the
704 cellular surface.

705 *S. flexneri* infection affects different host endocytic pathways

706 Next, we investigated whether *S. flexneri* directly blocked the
707 endocytic pathways. In the first instance, we aimed to test *S.*
708 *flexneri* infection on clathrin-dependent endocytosis (CDE). To
709 do this, we performed Tf uptake experiments using Tf, a *bona fide*
710 cargo of CDE (19). Hep2 cells were either left uninfected or were
711 infected for 90 min with GFP-WT *S. flexneri*, prior to incubation
712 with Tf-AF647 at 37°C for different time-points, and followed by
713 FC analysis. In WT-infected cells, we observed a 54% reduction
714 in the endocytosis rate, as well as a significant inhibition of the
715 total Tf uptake at the 30 minutes end-point (Fig. 3A-B), which
716 was independent of the surface expression of TfR (Fig. S3A). This
717 defect on Tf uptake was also observed in WT-infected polarized
718 Caco-2/TC7 cells, after basolateral incubation with fluorescent Tf
719 (Figs. S3C-D). In order to test if other endocytic pathways were
720 affected by *S. flexneri* infection, we assayed for IL-2 receptor (IL-
721 2R) uptake, a well-described marker of a clathrin-independent
722 endocytosis (CIE) pathway (20). Hep2 β cells, stably expressing the
723 IL-2R β chain, were left uninfected or infected with WT *S.*
724 *flexneri* strain for 90 min and then incubated with an anti-IL-2R β
725 chain antibody coupled to Cy3 for 15 min, fixed and analyzed by
726 fluorescent microscopy (21) (Fig. 3C). We observed a dramatic
727 reduction in IL-2R β uptake in WT-infected cells after 15 min
728 of endocytosis when compared to uninfected cells (Fig. 3D).
729 These results indicate that WT *S. flexneri* reduces both clathrin-
730 dependent and -independent endocytosis pathways.

731 As IpaJ and VirA effectors target key players in regulating
732 intracellular transport, we asked whether they had an impact
733 on this inhibition of endocytosis. Thus, we infected cells with *S.*
734 *flexneri* WT, *virA*, *ipaJ* and *virAipaJ* strains and performed Tf-
735 AF647 uptake kinetics. We observed a partial recovery of Tf
736 uptake when infecting cells with the three mutant strains (Fig.
737 3B), indicating that both IpaJ and VirA decrease endocytosis.
738 This IpaJ/VirA-dependent Tf endocytosis inhibition is stronger
739 than BFA, which does not induce significant changes in contrast to
740 uninfected conditions (Fig. 3B), as previously reported (17, 22).
741 In addition, we confirmed that the inhibitory effect of IpaJ and VirA
742 on endocytosis was due to their catalytic activities, as their ectopic
743 expression in Hep2 cells considerably decreased Tf uptake but
744 not when their catalytic-inactive forms were expressed (Fig. 3E).
745 In order to determine whether other effectors were involved in
746 the Tf uptake impairment, we next tested a panel of *S. flexneri*
747 mutants lacking effectors with different cellular targets (Figs. 3B,

748 S3B). Interestingly, we also found a partial recovery of Tf uptake
749 in cells infected with the *ipaA* mutant, which lacks the vinculin-
750 binding protein IpaA (Fig. 3B) (23). Again, the differences in
751 Tf uptake rate between mutant strains and WT could not be
752 explained by differences of TfR surface expression (Fig. S3A).
753 Overall, these results demonstrate that three *S. flexneri* effectors,
754 IpaJ, VirA and IpaA, inhibit endocytosis in the host cell.
755

756 To gain more insight into the mechanisms by which *S. flexneri*
757 affects CDE and CIE, we looked at dynamin 2 (Dnm2), an
758 enzyme implicated in both pathways and involved in the pinching-
759 off of vesicles from the plasma membrane (24). To this end, we left
760 uninfected or infected Hep2 β Dnm2-GFP genome-edited cells
761 (25) with WT *S. flexneri* and analyzed the Dnm2-GFP distribution
762 at plasma membrane by total internal reflection fluorescence
763 (TIRF) microscopy (Fig. 3F-G). Upon WT-infection, we observed
764 a 27% reduction of Dnm2-GFP at the plasma membrane (Fig.
765 3F), which was quantified by image analysis (Fig. 3G). This re-
766 duction was not due to a decrease of total Dnm2-GFP levels (Fig.
767 S3E), but likely linked to a reduced recruitment of Dnm2-GFP
768 to the plasma membrane and hence to endocytic sites. Similar
769 results were obtained when we analyzed the clathrin light chain
770 A (CLC) behavior in Hep2 β CLC-GFP genome-edited cells (25)
771 (Fig. S3F-G). Interestingly, this phenotype was correlated with
772 IpaJ and VirA expression since cells infected with either the single
773 or the double *virAipaJ* mutants recovered the normal Dnm2-GFP
774 and CLC-GFP recruitment at the plasma membrane (Figs. 3G,
775 S3G). In addition, BFA-treated cells also showed a reduction in
776 Dnm2-GFP at the plasma membrane, although smaller than upon
777 infection with WT bacteria (Fig. 3G). In contrast, IpaA led to
778 a marginal effect on Dnm2-GFP distribution (Fig. 3G). These
779 results indicate that Dnm2, a key host factor involved in both
780 CDE and CIE, is affected by *S. flexneri*, explaining the observed
781 reduction in the uptake of both Tf and IL-2R upon infection.
782 Altogether, our results show how IpaJ and VirA effectors induce
783 multifactorial defects on the general intracellular trafficking of
784 host cells.

785 IpaJ and VirA disorganize cell polarity and colonic tissue 786 structure

787 According to our results, IpaJ and VirA are responsible for
788 blocking three intracellular trafficking pathways: secretion, recy-
789 cling and endocytosis. We therefore asked whether this vesicular
790 trafficking blockage affected the maintenance of cell polarity.
791 Therefore, we infected polarized Caco-2/TC7 cells and stained the
792 surface TfR, which is usually expressed in the basolateral
793 domain of polarized cells. We observed a pool of the TfR lo-
794 calizing at the apical cell domain upon WT *S. flexneri* infection,
795 similarly to what has been previously reported in BFA-treated
796 cells (26) (Fig. 4A). On the contrary, the TfR did not localize at
797 the apical domain of uninfected or *virAipaJ*-infected cells (Fig.
798 4A). These results indicate that IpaJ and VirA lead to a loss in
799 the polarized transport of TfR, hence highlighting the *S. flexneri*-
800 mediated disorganization of epithelial polarity.

801 We next asked whether these two effectors, by disrupting cell
802 polarity and epithelial barrier integrity, promoted new invasion
803 events in a second round of bacterial infection (Figs. 4B, S4A).
804 For that, we first infected cells with either GFP-expressing WT
805 or *virAipaJ* strains, and then with the same strains but expressing
806 dsRed. We then quantified the percentage of cells co-infected by
807 the GFP and dsRed strains (Figs. 4B, S4A). We observed that
808 cells primo-infected with the WT strain were more prone to be re-
809 infected with either the WT or the *virAipaJ* strain when comparing
810 with *virAipaJ* primo-infected cells, which were poorly re-infected
811 (Fig. 4B). This result indicates that IpaJ and VirA favor multiple
812 invasion events, thereby enhancing the efficiency of infection.
813

814 Next, we used an *in vivo* model of infection to analyze whether
815 the trafficking impairment caused by IpaJ and VirA induced
816 changes in the colonic epithelial structure and function. We in-

817 fected Guinea pigs intrarectally (27, 28) with *S. flexneri* WT or
818 the double mutant *virAipaJ*. First, we observed a compact Golgi
819 structure in colonocytes from *virAipaJ*-infected animals as com-
820 pared to a fragmented Golgi apparatus observed in WT infected
821 animals, confirming the combined action of IpaJ and VirA on
822 disrupting Golgi structure *in vivo* (Fig. S4B). We then analyzed
823 the relative depth penetration of WT and *virAipaJ* strains from
824 the epithelial surface within the colonic tissue (Figs. 4C-D, S4B).
825 We observed and quantified a 40% decrease in the penetration
826 depth of the *virAipaJ* mutant in contrast to the WT strain. This
827 difference cannot be explained by a spreading defect in the
828 *virAipaJ* mutant, as the plaques formed on a cell monolayer by the
829 *virAipaJ* mutant after 48 hours of infection are only 3% smaller
830 than the ones formed by the WT strain (Fig. S4C). Overall,
831 these results indicate that IpaJ and VirA, by the induction of a
832 general trafficking impairment, are critical for intestinal epithelial
833 invasion *in vivo*.

834 Discussion

835 In this study, we showed how two *S. flexneri* effectors, IpaJ and
836 VirA, are necessary and sufficient to block several key intracellu-
837 lar trafficking pathways in invaded cells, inducing a “frozen” state
838 in which cells are no longer able to exchange molecules with their
839 environment. These results were observed *in vitro* both in non-
840 polarized and polarized cells. Moreover, we were able to show *in*
841 *in vivo* the impact of some of the functions of these effectors on the
842 efficient intestinal invasion by the bacteria.

843 Our work confirmed, in the context of cellular *S. flexneri* infec-
844 tion, the secretion blockage described when overexpressing either
845 of the effectors, IpaJ or VirA (10, 13). This is not trivial as EspG
846 for instance, the enterohaemorrhagic and enteropathogenic *Es-*
847 *cherichia coli* (EHEC/EPEC) homolog of *Shigella* VirA, does not
848 affect the secretory transport during EHEC infection (29), but
849 only during ectopic overexpression. This suggests that Rab1 is
850 not targeted *in vivo* by EHEC EspG, and illustrates how the
851 overexpression of certain virulence factors might induce pheno-
852 types that are not observed during natural infection. However,
853 the fact that VirA blocks the secretory transport in *S. flexneri*-
854 infected cells strongly suggests that Rab1 is a VirA substrate,
855 but does not exclude the possibility that other Rabs might be
856 targeted by this effector. In line with this, we demonstrated that
857 VirA, in combination with IpaJ, impairs the normal recycling
858 of cell receptors. VirA, in contrast to EPEC/EHEC EspG, was
859 shown *in vitro* to have a broader range of specificity towards Rab
860 GTPases (13). This strongly suggests that endosomal Rabs, such
861 as Rab11, Rab35 or Rab22 (30), are targeted and inactivated by
862 VirA, explaining part of the recycling impairment. Interestingly,
863 it was reported that EspG reduces surface receptor levels and
864 receptor recycling in EHEC infected cells (29) and this is due to
865 the modulation of an Arf6:Rab35 signaling axis (31). Moreover,
866 EspG was shown to interact with Arf GTPases and PAK (13, 32).
867 However, unlike in EHEC infection, a scaffolding role of VirA
868 modulating Rab-Arf signaling has not been described so far for *S.*
869 *flexneri*. On the other hand, our results show that IpaJ and VirA
870 work in concert to induce an additive defect in receptor recycling.
871 Although IpaJ activity slows down Tf recycling by targeting Arf1,
872 this might also happen via the inactivation of other Arf family
873 members (11, 33). Altogether, our work reveals that in the case
874 of *S. flexneri* infection, both IpaJ and VirA are necessary to induce
875 strong recycling inhibition by acting on Arf GTPases and possibly
876 on Rab GTPases.

877 The targeting of the endosomal compartments by these two
878 effectors has consequences not only restricted to the surface
879 receptor recycling, but also to an endocytosis blockage. How IpaJ
880 and VirA reduce Tf uptake, as well as dynamin 2 and clathrin
881 recruitment to endocytic sites at the plasma membrane remains
882 a key question. One hypothesis is that the concerted action of

883 these two effectors on the secretory and recycling pathways will
884 induce downstream alterations on the endocytic route, as the
885 intracellular trafficking routes are intimately interlinked. Indeed,
886 these two *S. flexneri* effectors target two families of proteins
887 that are key regulators of many intracellular trafficking events,
888 possibly explaining the endocytosis impairment as an indirect
889 consequence of their activities on small GTPases. One possibility
890 suggested by our results is that impairment of exocytosis pathways
891 by IpaJ and VirA blocks the recruitment of dynamin 2 to the
892 plasma membrane. Interestingly, this inhibition is also observed
893 upon BFA treatment, which targets only Arf proteins. However,
894 the effect of BFA being less strong than *Shigella* infection might
895 explain why this drug does not significantly decrease Tf endo-
896 cytosis and further suggests that the combined action of IpaJ
897 and VirA on Arf and Rab proteins is needed to strongly affect
898 endocytosis. Moreover, it was also reported that dynamin 2 is
899 recruited to the budding sites of recycling endosomes, as well as
900 to the TGN (34, 35), possibly explaining the decreased dynamin
901 2 recruitment upon *S. flexneri* infection. The bacterium might
902 also affect endocytosis by targeting actin, an important factor for
903 dynamin 2 recruitment (36, 37), since it possesses several effec-
904 tors modulating actin polymerization, such as IpaC, IcsA, and
905 IpaA (38). In agreement with this, our results demonstrated that
906 IpaA, a vinculin-binding protein involved in actin reorganization,
907 partially inhibits endocytosis. Moreover, the plasma membrane
908 tension, which is regulated by actin polymerization, was shown
909 to affect endocytosis dynamics in polarized cells (39). Thus, by
910 targeting actin dynamic regulators, *S. flexneri* might modulate the
911 plasma membrane tension thereby inhibiting the endocytosis rate
912 of the host cell.

913 Finally, the global secretion inhibition determined by our
914 proteomic approach revealed a list of less secreted proteins that
915 participate in cell polarity establishment and differentiation (40)
916 and their modulation by *S. flexneri* might perturb the integrity of
917 the intestinal barrier. Candidates among such proteins are those
918 regulating cell adhesion, ECM composition and lipid transport. In
919 addition, the impairment in the secretion of immunomodulators
920 might affect the host immune response. Moreover, our *in vitro*
921 data show that IpaJ and VirA subvert the epithelial polarity
922 and promote multiple invasion events, and we have preliminary
923 data suggesting that they might regulate intercellular junctions
924 stability. These results are in total agreement with our *in vivo*
925 data showing that IpaJ and VirA induce a deeper *S. flexneri*
926 penetration into the colonic tissue.

927 Overall, our work shows how *S. flexneri* IpaJ and VirA effec-
928 tors coordinate and modulate the host cell intracellular traffick-
929 ing, leading to the subversion of the infected cells and tissue that
930 will result in more efficient bacterial invasion.

931 Acknowledgments

932 We are very grateful to Pierre-Henri Commere (PFC, Cytometry Platform
933 of Institut Pasteur) for technical help with the FACS MoFlo Astrios EQ, Gaëlle
934 Boncompain and Frank Perez for RUSH reagents, Laurie Pinaud and Claude
935 Parsot for sharing reagents and helpful discussion and to Katja Brunner
936 for critical reading of the manuscript. We thank PBI (Imagopole) platform of
937 Institut Pasteur for microscope maintenance and technical help. This project
938 was funded by ERC Advanced Grants 232798 and 339579 to PJS, FRM grant
939 to MLF (SPF20121226366), PTR 22-16 grant to AG, “Région Ile-de-France”
940 and Fondation pour la Recherche Médicale grants to DL. LS is part of the
941 Pasteur Paris University (PPU) International PhD Program and has received
942 funding from the European Union’s Horizon 2020 research and innovation
943 programme under the Marie Skłodowska-Curie grant agreement No 665807.
944 **Author contribution** MLF, NS and PJS conceived and designed research. MLF
945 and VM performed most of the experiments. AG participated on TIRFM
946 experiments and LS on IL-2R endocytosis and colocalization analysis. GN
947 performed *in vivo* experiments with MLF. SDL participated on MS post-
948 analysis. JRR and PS generated *virAipaJ* and *ospC1C2C3* mutant strains,
949 respectively. VMasson carried out the MS experimental work, GA analyzed
950 MS data and DL supervised MS and data analysis. MLF and NS wrote the
951 manuscript with the input of all authors. NS and PJS supervised the project.

953
954
955
956
957
958
959
960
961
962
963
964
965
966
967
968
969
970
971
972
973
974
975
976
977
978
979
980
981
982
983
984
985
986
987
988
989
990
991
992
993
994
995
996
997
998
999
1000
1001
1002
1003
1004
1005
1006
1007
1008
1009
1010
1011
1012
1013
1014
1015
1016
1017
1018
1019
1020

1. Donaldson JG, Jackson CL (2011) ARF family G proteins and their regulators: roles in membrane transport, development and disease. *Nat Rev Mol Cell Biol* 12(6):362–75.
2. Barr F a (2013) Review series: Rab GTPases and membrane identity: causal or inconsequential? *J Cell Biol* 202(2):191–9.
3. Hutagalung AH, Novick PJ (2011) Role of Rab GTPases in Membrane Traffic and Cell Physiology. *Physiol Rev* 91(1):119–149.
4. Phalipon A, Sansonetti PJ (2007) Shigella 's ways of manipulating the host intestinal innate and adaptive immune system : a tool box for survival ? (September 2006):119–129.
5. Galán JE, Lara-Tejero M, Marlovits TC, Wagner S (2014) Bacterial Type III Secretion Systems: Specialized Nanomachines for Protein Delivery into Target Cells. *Annu Rev Microbiol* 68(1):415–438.
6. Schroeder GN, Hilbi H (2008) Molecular pathogenesis of Shigella spp.: controlling host cell signaling, invasion, and death by type III secretion. *Clin Microbiol Rev* 21(1):134–56.
7. Ashida H, Mimuro H, Sasaki C (2015) Shigella manipulates host immune responses by delivering effector proteins with specific roles. *Front Immunol* 6(MAY). doi:10.3389/fimmu.2015.00219.
8. Parsot C (2009) Shigella type III secretion effectors: how, where, when, for what purposes? *Curr Opin Microbiol* 12(1):110–6.
9. Mounier J, et al. (2012) Shigella Effector IpaB-Induced Cholesterol Relocation Disrupts the Golgi Complex and Recycling Network to Inhibit Host Cell Secretion. *Cell Host Microbe* 12(3):381–9.
10. Burnaevskiy N, et al. (2013) Proteolytic elimination of N-myristoyl modifications by the Shigella virulence factor IpaJ. *Nature* 1:1–17.
11. Burnaevskiy N, Peng T, Reddick LE, Hang HC, Alto NM (2015) Myristoylome profiling reveals a concerted mechanism of ARF GTPase deacylation by the bacterial protease IpaJ. *Mol Cell* 58(1):110–122.
12. Dobbs N, et al. (2015) STING activation by translocation from the ER is associated with infection and autoinflammatory disease. *Cell Host Microbe* 18(2):157–168.
13. Dong N, et al. (2012) Structurally distinct bacterial TBC-like GAPs link Arf GTPase to Rab1 inactivation to counteract host defenses. *Cell* 150(5):1029–1041.
14. Campbell-Volais FX, Sachse M, Sansonetti PJ, Parsot C (2015) Escape of actively secreting shigella flexneri from ATG8/LC3-Positive vacuoles formed during cell-to-cell spread is facilitated by IcsB and VirA. *MBio* 6(3):1–11.
15. Boncompain G, et al. (2012) Synchronization of secretory protein traffic in populations of cells. *Nat Methods* 9(5):493–8.
16. Ong S-E, et al. (2002) Stable Isotope Labeling by Amino Acids in Cell Culture, SILAC, as a Simple and Accurate Approach to Expression Proteomics. *Mol Cell Proteomics* 1(5):376–386.
17. Lippincott-Schwartz J, et al. (1991) Brefeldin A's effects on endosomes, lysosomes, and the TGN suggest a general mechanism for regulating organelle structure and membrane traffic. *Cell* 67(3):601–16.
18. De Figueiredo P, et al. (2001) Inhibition of Transferrin Recycling and Endosome Tubulation by Phospholipase A2Antagonists. *J Biol Chem* 276(50):47361–47370.
19. Robinson MS (2015) Forty Years of Clathrin-coated Vesicles. *Traffic* 16(12):1210–1238.
20. Lamaze C, et al. (2001) Interleukin 2 receptors and detergent-resistant membrane domains define a clathrin-independent endocytic pathway. *Mol Cell* 7(3):661–671.
21. Basquin C, et al. (2015) Membrane protrusion powers clathrin-independent endocytosis of interleukin-2 receptor. *EMBO J* 34(16):1–15.
22. Hunziker W, Andrew Whitney J, Mellman I (1991) Selective inhibition of transcytosis by brefeldin A in MDCK cells. *Cell* 67(3):617–627.
23. Tran Van Nhieu G, Ben-Ze'ev A, Sansonetti PJ (1997) Modulation of bacterial entry into epithelial cells by association between vinculin and the Shigella IpaA invasin. *EMBO J* 16(10):2717–2729.
24. Antony B, et al. (2016) Membrane fission by dynamin: what we know and what we need to know. *EMBO J*. doi:10.15252/embj.201694613.
25. Bertot L, et al. (2018) Quantitative and Statistical Study of the Dynamics of Clathrin-Dependent and -Independent Endocytosis Reveal a Differential Role of EndophilinA2. *Cell Rep* 22(6):1574–1588.
26. Wang E, Pennington JG, Goldenring JR, Hunziker W, Dunn KW (2001) Brefeldin A rapidly disrupts plasma membrane polarity by blocking polar sorting in common endosomes of MDCK cells.
27. Arena ET, et al. (2015) Bioimage analysis of Shigella infection reveals targeting of colonic crypts. *Proc Natl Acad Sci* 112(25):E3282–E3290.
28. Shim D-H, et al. (2007) New Animal Model of Shigellosis in the Guinea Pig: Its Usefulness for Protective Efficacy Studies. *J Immunol* 178(4):2476–2482.
29. Clements A, Stoneham CA, Furniss RCD, Frankel G (2014) Enterohaemorrhagic Escherichia coli inhibits recycling endosome function and trafficking of surface receptors. *Cell Microbiol* 16(11):1693–1705.
30. Grant BD, Donaldson JG (2009) Pathways and mechanisms of endocytic recycling. *Nat Rev Mol Cell Biol* 10(9):597–608.
31. Furniss RCD, Slater S, Frankel G, Clements A (2016) Enterohaemorrhagic E. coli modulates an ARF6:Rab35 signaling axis to prevent recycling endosome maturation during infection. *J Mol Biol* 428(17):3399–3407.
32. Selyunin AS, et al. (2011) The assembly of a GTPase-kinase signalling complex by a bacterial catalytic scaffold. *Nature* 469(7328):107–111.
33. Volpicelli-Daley LA, Li Y, Zhang C, Kahn RA (2005) Isoform-selective Effects of the

Bacterial strains

Shigella flexneri 5a strain M90T, harboring a streptomycin resistance mutation (41), was used as the WT strain. All the mutants from this study were generated from the WT strain. All the mutant strains used in this study were part of a *S. flexneri* mutant collection (42), except: *ipgD* (43), *virAipA*, *ospE1E2* and *ospC1C2C3*. Tetracycline resistance cassette was removed from *virA* strain to avoid reduction in IcsA protein levels by FLP-FRT recombination using the pCP20 plasmid. Frozen bacterial stocks

34. Depletion of ADP-Ribosylation Factors 1–5 on Membrane Traffic. 16(October):4495–4508.
34. van Dam EM, Stoorvogel W (2002) Dynamin-dependent Transferrin Receptor Recycling by Endosome-derived Clathrin-coated Vesicles. *Mol Biol Cell* 13(1):169–182.
35. Cao H, et al. (2005) Actin and Arf1-dependent recruitment of a cortactin-dynamin complex to the Golgi regulates post-Golgi transport. *Nat Cell Biol*. doi:10.1038/ncb1246.
36. Taylor MJ, Lampe M, Merrifield CJ (2012) A feedback loop between dynamin and actin recruitment during clathrin-mediated endocytosis. *PLoS Biol*. doi:10.1371/journal.pbio.1001302.
37. Grassart A, et al. (2014) Actin and dynamin2 dynamics and interplay during clathrin-mediated endocytosis. *J Cell Biol*. doi:10.1083/jcb.201403041.
38. Valencia-Gallardo CM, Carayol N, Tran Van Nhieu G (2015) Cytoskeletal mechanics during Shigella invasion and dissemination in epithelial cells. *Cell Microbiol* 17(2):174–182.
39. Boulant S, Kural C, Zeeh JC, Ubelmann F, Kirchhausen T (2011) Actin dynamics counteract membrane tension during clathrin-mediated endocytosis. *Nat Cell Biol*. doi:10.1038/ncb2307.
40. García-Lorenzo A, Rodríguez-Piñero AM, Rodríguez-Berrocal FJ, de la Cadena MP, Martínez-Zorzano VS (2012) Changes on the Caco-2 secretome through differentiation analyzed by 2-D differential in-gel electrophoresis (DIGE). *Int J Mol Sci* 13(11):14401–14420.
41. Allaoui A, Sansonetti PJ, Parsot C (1992) MxiJ, a lipoprotein involved in secretion of Shigella Ipa invasins, is homologous to YscJ, a secretion factor of the Yersinia Yop proteins. *J Bacteriol* 174(23):7661–7669.
42. Sidik S, et al. (2014) A Shigella flexneri Virulence Plasmid Encoded Factor Controls Production of Outer Membrane Vesicles. *G3&#amp;#58; Genes|Genomes|Genetics* 4(12):2493–2503.
43. Allaoui A, Menard R, Sansonetti PJ, Parsot C (1993) Characterization of the Shigella flexneri ipgD and ipgF genes, which are located in the proximal part of the mxi locus. *Infect Immun* 61(5):1707–1714.
44. Grassart A, Dujeancourt A, Lazarow PB, Dautry-Varsat A, Sauvonnnet N (2008) Clathrin-independent endocytosis used by the IL-2 receptor is regulated by Rac1, Pak1 and Pak2. *EMBO Rep* 9(4):356–362.
45. Fourriere L, Divoux S, Roceri M, Perez F, Boncompain G (2016) Microtubule-independent secretion requires functional maturation of Golgi elements. *J Cell Sci* 129(17):3238–3250.
46. Labigne-Roussel AF, Lark D, Schoolnik G, Falkow S (1984) Cloning and expression of an afimbrial adhesin (AFA-I) responsible for P blood group-independent, mannose-resistant hemagglutination from a pylonophytic Escherichia coli strain. *Infect Immun*.
47. Valdivia RH, Falkow S (1996) Bacterial genetics by flow cytometry: Rapid isolation of Salmonella typhimurium acid-inducible promoters by differential fluorescence induction. *Mol Microbiol* 22(2):367–378.
48. Sörensen M, et al. (2003) Rapidly maturing red fluorescent protein variants with strongly enhanced brightness in bacteria. *FEBS Lett* 552(2–3):110–114.
49. Campbell-Volais F-X, et al. (2014) A fluorescent reporter reveals on/off regulation of the Shigella type III secretion apparatus during entry and cell-to-cell spread. *Cell Host Microbe* 15(2):177–89.
50. Poulet P, Carpentier S, Barillot E (2007) myProMS, a web server for management and validation of mass spectrometry-based proteomic data. *Proteomics* 7(15):2553–2556.
51. Valot B, Langella O, Nano E, Zivy M (2011) MassChroQ: A versatile tool for mass spectrometry quantification. *Proteomics* 11(17):3572–3577.
52. Ritchie M, et al. (2015) limma powers differential expression analyses for RNA-sequencing and microarray studies. *Nucleic Acids Res* 43(7):e47.
53. Benjamini Y, Hochberg Y, Benjamini, Y. and Hochberg Y (1995) Controlling the false discovery rate: a practical and powerful approach to multiple testing. *J R Stat Soc Ser B Methodol* 57(1):289–300.
54. Vizcaino JA, et al. (2016) 2016 update of the PRIDE database and its related tools. *Nucleic Acids Res* 44(D1):D447–D456.
55. Kowal J, et al. (2016) Proteomic comparison defines novel markers to characterize heterogeneous populations of extracellular vesicle subtypes. *Proc Natl Acad Sci* 113(8):E968–E977.
56. Petersen TN, Brunak S, Von Heijne G, Nielsen H (2011) SignalP 4.0: Discriminating signal peptides from transmembrane regions. *Nat Methods*. doi:10.1038/nmeth.1701.
57. Bendtsen JD, Jensen LJ, Blom N, Von Heijne G, Brunak S (2004) Feature-based prediction of non-classical and leaderless protein secretion. *Protein Eng Des Sel*. doi:10.1093/protein/gzh037.
58. Ashburner M, et al. (2000) Gene ontology: Tool for the unification of biology. *Nat Genet* 25(1):25–29.
59. Thomas PD, et al. (2003) PANTHER: A library of protein families and subfamilies indexed by function. *Genome Res*. doi:10.1101/gr.772403.
60. Schindelin J, et al. (2012) Fiji: An Open-Source Platform for Biological- Image Analysis. *Nat Methods* 9(June 2012):676–682.
61. De Chaumont F, et al. (2012) Icy: An open bioimage informatics platform for extended reproducible research. *Nat Methods*. doi:10.1038/nmeth.2075.
62. Lagache T, et al. (2018) Mapping molecular assemblies with fluorescence microscopy and object-based spatial statistics. *Nat Commun* 9(1):102–108.

Methods

were streaked onto trypticase soy agar (TSA) plates containing 0.1% (w/v) Congo red (CR) and grown at 37 °C overnight. Plates were kept at 4 °C for up to two weeks.

Cell lines

Hep2 cells (HeLa derivative) and its derivatives expressing the β -chain of IL-2R, Hep2 β , were grown in DMEM 1 g/L (Gibco™) supplemented with 10% heat-inactivated fetal calf serum (HI-FCS, Eurobio) at 5% CO₂ at 37° C (44), in the presence of 1 mg/mL G418 (Sigma) for Hep2 β cells. CRISPR-Cas9 genome edited Hep2 β Dnm2-

1021
1022
1023
1024
1025
1026
1027
1028
1029
1030
1031
1032
1033
1034
1035
1036
1037
1038
1039
1040
1041
1042
1043
1044
1045
1046
1047
1048
1049
1050
1051
1052
1053
1054
1055
1056
1057
1058
1059
1060
1061
1062
1063
1064
1065
1066
1067
1068
1069
1070
1071
1072
1073
1074
1075
1076
1077
1078
1079
1080
1081
1082
1083
1084
1085
1086
1087
1088

1089 GFP and Hep2β CLC-GFP cells (25), and the RUSH stable HeLa cell line expressing
 1090 the ER molecular hook Streptavidin-KDEL and the cargo SBP-EGFP-TNFα (45) were
 1091 described previously. Hep2 and HeLa cells are non-polarized cell, and were always
 1092 cultured to 70% confluence prior to infection experiments. Caco-2/TC7 cells (a clone
 1093 of Caco-2 cells, human colorectal adenocarcinoma origin) were grown in DMEM
 1094 1 g/L supplemented with 20% HI-FCS, GlutaMAX™ and non-essential amino acids
 1095 (Gibco™). For complete polarization and differentiation of Caco-2/TC7 cells, 2x10⁵
 1096 cells/cm² cells were seeded into 12-well or 6-well Transwell inserts (pore size 0.4
 1097 μm, Corning) and cultured for 18-21 days at 10% CO₂ at 37° C; fresh media was
 1098 added triweekly, except for plaque assay experiments, where cells were cultured
 1099 on plastic 6-well plates. Transepithelial electrical resistance (TEER) was measured
 1100 using a Millicell-ERS Volt-ohm meter (Millipore). Dextran permeability was assessed
 1101 by adding 70 kDa FITC-Dextran 200 μg/mL (Sigma) in Ringer's buffer to the apical
 1102 compartment of Transwell inserts (uninfected or infected in Ringer's solution: 155
 1103 mM NaCl, 3 mM KCl, 3 mM NaH₂PO₄, 5 mM Hepes 10 mM Glucose, pH 7.0, with 2
 1104 mM CaCl₂, 1 mM MgCl₂) after a 15 min preincubation in Ringer's buffer or in calcium-
 1105 free Ringer's (containing 10 mM glucose). Fluorescence pass-through to the basal
 1106 compartment medium was measured with an Infinite M200 Pro multimode plate-
 1107 reader (TECAN). Lactate dehydrogenase (LDH) was quantified with the CytoTox 96®
 1108 Non-Radioactive Cytotoxicity Assay (Promega).

Plasmids
 1109 Bacteria transformed with plasmids coding for the *Escherichia coli* AfaE adhesin (46),
 1110 or GFP (pFPV 25.1) (47), dsRed (48) or mCherry fluorescent proteins, were used as
 1111 indicated. pTRIO-mCherry plasmid was generated by inserting mCherry CDS in *Xmal*-
 1112 *NheI* sites of pTRIO plasmid, which is the basic backbone of the pTSAR plasmids series
 1113 (49). The CDS of *ipaJ* was cloned through *EcoRI-BamHI* into pSU2.1tt plasmid (49),
 1114 giving the pSU2.1tt-*ipaJ*-Myc plasmid. The catalytic site variant was generated by
 1115 PCR-based mutagenesis introducing the C64A mutation into *ipaJ* (plasmid pSU2.1tt-
 1116 *ipaJ*-C64A-Myc). *ipaJ* and *virAipaJ* mutant strains were complemented with pSU2.1tt-
 1117 *ipaJ*-Myc or pSU2.1tt-*ipaJ*-C64A-Myc plasmids. pSU2.1tt-*VirA*-Myc or pSU2.1tt-*VirA*-
 1118 RQ-Myc plasmids (14) were used to complement *virAipaJ* or *virA* strains. For the
 1119 ectopic expression of GFP-*VirA*, GFP-*ipaJ* and their mutated variants in mammalian
 1120 cells, the CDS of *ipaJ* and *virA* were cloned through *HindIII-KpnI* into pEGFP-C1
 1121 plasmid.

Antibodies and reagents
 1122 The following primary antibodies were used: rabbit anti-*S. flexneri* 5a M90T LPS
 1123 1:300, mouse anti-GM130 1:200 (BD, #610823), rabbit anti-GM130 1:100 (Abcam,
 1124 ab52649), mouse anti-GFP DyLight 680 1:1000 (Rockland, #600-144-215), mouse anti-
 1125 ERGIC53 1:100 (Sigma, SAB4200585), rabbit anti-Sec24b 1:100 (D7D65) (Cell Signaling
 1126 Technology, #12042), sheep anti-TGN46 1:100 (Bio-Rad, AHP500GT), purified mouse
 1127 mAb OKT9 (anti-TfR) 1:100, goat anti-dynamin-2 1:500 (Santa Cruz, sc-6400), rabbit
 1128 anti-clathrin LCA (H-55) 1:500 (Santa Cruz, sc-28276), rabbit anti-GFP 1:1000 (Rock-
 1129 land, #600-401-215), rabbit anti-actin 1:5000 (Sigma, A2066), chicken anti-GFP 1:1000
 1130 (Abcam, ab13970). All the secondary antibodies were from all from Molecular Probes
 1131 and used at 1:500 dilution. FITC-Dextran 70 (Sigma, #46945), Dapi 1 μg/mL (Sigma).
 1132 Phalloidin-AF647 1:100 (A22287, Molecular Probes). Brefeldin A (Sigma, B7651) was
 1133 used at 1 μg/mL.

Bacterial infections of cultured cells
 1134 Hep2 and Hep2β cells were plated the day before the experiment onto 12-mm
 1135 coverslips at a density of 0.4x10⁵ cells/cm² for immunofluorescence, or on glass
 1136 bottom dishes (Mattek) for total internal reflection fluorescence (TIRF) microscopy
 1137 experiments, and at a density of 0.4x10⁵ cells/cm² on 6-well plates for flow cytometry
 1138 (FC) or western blot experiments. Bacterial cultures were prepared by picking a
 1139 single colony from each strain from TSA-CR plates and grown in 8 mL of trypticase
 1140 soy broth (TSB) supplemented with the appropriate antibiotics (ampicillin 100 μg/mL,
 1141 chloramphenicol 10 μg/mL) in a shaking incubator overnight at 30 °C. Bacteria were
 1142 sub-cultured in fresh 8 mL TSB at 37° C until OD₆₀₀ 0.8 – 1.0, pelleted, washed in
 1143 PBS and coated with poly-L-lysine (mol wt 70,000 – 100,000, Sigma) 10 μg/mL in
 1144 PBS for 10 min, washed twice with PBS and resuspended in the infection medium
 1145 (DMEM supplemented with 20 mM Hepes) to the adequate multiplicity of infection
 1146 (MOI). Coated bacteria were added to the cells and allowed to adhere for 15 min at
 1147 room temperature (RT), and then incubated at 37° C in a CO₂ incubator or in a water
 1148 bath when short time of infection or short kinetics were performed. For infections of
 1149 Caco-2/TC7 cells grown in transwell filters, AfaE-expressing strains were cultured as
 1150 described, pelleted, washed with PBS and resuspended in infection medium to the
 1151 adequate MOI. Apical and basal chambers were washed twice with warm DMEM-
 1152 Hepes and bacteria were added to the apical chamber at a MOI = 75, incubated for
 1153 15 min at RT and switched to a 37 °C CO₂ incubator. After 30 min, the medium was
 1154 aspirated and replaced for fresh DMEM-Hepes supplemented with gentamicin 50
 1155 μg/mL and incubated for the indicated additional time.
 1156 For plaque assays, Caco-2/TC7 cell monolayers were cultured on plastic 6-well plates
 for 3 weeks, infected at a MOI of 5 for 2 hours, washed and followed by the addition
 of a 0.5% agarose overlay containing 50 μg/mL gentamicin in culture medium. 48
 hours later, cells were fixed with ethanol and stained with Giemsa R solution. Plaque
 sizes were quantified using Fiji (Image J) software.

RUSH assay to assess anterograde trafficking
 RUSH stable HeLa cell line expressing the ER molecular hook Streptavidin-KDEL and
 the cargo SBP-EGFP-TNFα (45) were uninfected or infected with the indicated *S.*
flexneri strain expressing mCherry fluorescent protein. After 15 min at RT and 45
 min at 37 °C, the medium was replaced by medium containing 40 μM of biotin
 (Sigma) to initiate the cargo transport from the ER and incubated at 37 °C for
 additional 60 min. Cells were washed with ice-cold PBS, fixed in PFA 4%-PBS for
 20 min on ice and stained for 1 hour at RT with an anti-GFP DyLight 680 antibody
 (Rockland) to detect the surface-arrived SBP-EGFP-TNFα. After harvesting, surface

anti-GFP DyLight 680 fluorescence was measured by FC (MoFlo Astrios EQ, Beckman)
 in the infected population of cells (mCherry positive). Results are the mean expressed
 as the percentage of total (uninfected or infected) cells expressing the RUSH cargo
 at their surface. Alternatively, cells grown on coverslips were infected as before and
 subsequent immunofluorescences were performed as indicated in the figures.

SILAC labeling, infections, sample collection and preparation
 Human Caco-2/TC7 cells were cultured for 6 passages in SILAC DMEM flex media
 deficient for L-arginine and L-lysine (Gibco) with 20% heat inactivated dialyzed FBS
 (dFBS) (Thermo Fischer), 1 g/L glucose (Sigma), GlutaMAX 1X, non essential amino
 acids, 10 U/mL penicillin/streptomycin (all from Gibco) supplemented with either
 13C6, 15N4 L-Arginine-HCl and 13C6, 15N2 L-Lysine-2HCl (Heavy media) or with 13C6
 L-Arginine-HCl and 4,4,5,5-D4 L-Lysine-2HCl (Medium media) (arginine at 84mg/mL
 and lysine at 146 mg/mL, Thermo Fisher Scientific). The stable isotope labeling was
 confirmed by LC-MS/MS after protein in-gel separation and digestion of blue bands.
 Labeled cells were seeded on 6-well Transwell inserts and cultured for 21 days in
 Heavy or Medium SILAC medium changing the medium 3 times per week.
 For secretome collection, 24 hours before infections cells were washed with DMEM
 for SILAC with 20 mM Hepes and medium was replaced with either Medium or Heavy
 SILAC media but containing 2% dFBS. Cells were uninfected or infected with AfaE-
 expressing WT or *virAipaJ* strains. To that end, apical and basal chambers of Transwell
 inserts were washed 3 times with DMEM for SILAC/Hepes, Medium SILAC medium
 was added to uninfected cells, and bacteria were added in the apical chamber at a
 MOI 75 in Heavy SILAC medium without FBS or antibiotics. After 15 min at RT and 30
 min at 37° C, cells were washed 3 times with DMEM for SILAC/Hepes, 1.5 mL of FBS-
 free Medium or Heavy SILAC media with 50 μg/mL gentamicin were added at either
 apical or basal Transwell chambers, and cells were further incubated at 37° C for 4 ½
 hours. Apical and basal secretomes were collected (total volume: 3.6 mL/condition),
 UI and infected samples mixed in a 1:1 ratio, centrifuged (200 x g, 5 min), filtered
 with 0.22 μm syringe filters (Minisart, Sartorius Stedim Biotech S.A.) and snap-frozen
 in liquid N₂. For proteome analysis, cells were lysed in RIPA buffer containing
 protease inhibition cocktail and samples were mixed at a protein stoichiometry ratio
 of UI:infected 1:1. Samples were kept at -80° C until use. Before trypsin digestion,
 uninfected and infected secretomes mixing at a 1:1 ratio was done according to cell
 number in Transwells from which the secretome was prepared (total volume = 3.6
 mL), and then concentrated to 500 μL on Amicon Ultra-15, 10000 molecular weight
 cutoff centrifugation filter units (Millipore). For the filter-aided sample preparation
 protocol (FASP), a total of 60 mg of urea and 16 μL of M dithiothreitol were added
 to 500 μL of concentrated secretome, the solution was mixed on a Nanosep (10 kDa,
 Pall) device, and was incubated at 57 °C for 15 min. The mixture was spun down
 and was washed two times with 500 μL of 2 M urea in 0.1 Tris/HCl pH 8.5. A total of
 100 μL of 0.05 M iodoacetamide was added and was incubated for 30 min at RT in
 the dark. Two washes with 25 mM ammonium bicarbonate were performed and the
 secretome was digested with 5 μg of trypsin / LysC (Promega) for 4 hours at 37 °C.
 The digested peptides were collected by centrifugation, and the filtrate was dried in
 a vacuum concentrator at room temperature and was re-dissolved in solvent A (2%
 acetonitrile, 0.1 % formic acid). Peptides were then subjected to LC/MS analysis.
 For proteome analysis, mixed proteins lysates were separated on 10% SDS-PAGE (Thermo
 Fisher Scientific) and were digested in-gel with trypsin / LysC (Promega) as described
 in standard protocols. Extracted peptides were dried in a vacuum concentrator at
 room temperature and were re-dissolved in solvent A (2% MeCN, 0.1% HCO₂H)
 before LC/MS analysis.

LC-MS/MS analysis
 For the analysis of cell lysates, peptides were separated by reverse-phase chromatog-
 raphy by using an UltiMate 3000 RSLCnano system coupled to an Orbitrap Fusion
 mass spectrometer (Q-OT-qIT, Thermo Fisher Scientific). Samples were loaded on a
 nanoViper C18 μ-precolumn (75μm x 2 cm, Acclaim PepMap, Thermo Scientific) at
 5 μL/min of solvent A. After a desalting of 8 min, the precolumn was switched on
 the C18 column (75μm x 50 cm; 3 μm, 100Å, Acclaim PepMap, Thermo Scientific)
 equilibrated in solvent A. Bound peptides were eluted using a 168 min four step
 linear gradient (from 5 to 6% (v/v) in one min, 6 to 9% in 18 min, 9 to 30% in 132
 min and 30 to 40% in 9 min) of solvent B (100% MeCN, 0.085% HCO₂H) at 60°C and
 a 300 nL/min flow rate.
 For the analysis of secretome samples, peptides were loaded on a C18 μ-precolumn
 (Thermo Scientific) at 20 μL/min in solvent A. After a desalting step for 3 min,
 the precolumn was switched on the C18 column (Thermo Scientific) equilibrated in
 solvent A and peptide were eluted with a 215 minute two step linear gradient of
 solvent B (from 5 to 20% (v/v) in 147 min and 20 to 40% in 65 min).
 We acquired Survey MS scans at a resolution set to a value of 120,000, with a mass
 range of m/z 400–1500 and a 4 × 10⁵ ion count target. Tandem MS was performed by
 isolation at 1.6 Th with the quadrupole, HCD fragmentation with normalized collision
 energy of 28, and rapid scan MS analysis in the ion trap. The MS² ion count target was
 set to 1 × 10⁴ and only those precursors with charge state from 2 to 7 were sampled
 for MS² acquisition. The instrument was run in top speed mode with 3 s cycles.

LC-MS/MS Data Processing and Protein Identification
 Data were acquired using the Xcalibur software (v 3.0) and the resulting spectra
 were interrogated by Sequest HT through Thermo Scientific Proteome Discoverer
 (v 2.1) with the SwissProt human database (012016). The mass tolerances in MS and
 MS/MS were set to 10 ppm and 0.6 Da, respectively. We set carbamidomethyl cysteine,
 oxidation of methionine, N-terminal acetylation, heavy ¹³C₆¹⁵N₂-Lysine (Lys8) and
¹³C₆¹⁵N₄-Arginine (Arg10), medium ²H₄-Lysine (Lys4) and ¹³C₆-Arginine (Arg6) as
 variable modifications. We set specificity of Trypsin digestion and allowed 2 missed
 cleavage sites.
 The resulting files were further processed by using myProMS (v 3.5) (50). The Sequest
 HT target and decoy search result were validated at 1% false discovery rate (FDR)

1157
 1158
 1159
 1160
 1161
 1162
 1163
 1164
 1165
 1166
 1167
 1168
 1169
 1170
 1171
 1172
 1173
 1174
 1175
 1176
 1177
 1178
 1179
 1180
 1181
 1182
 1183
 1184
 1185
 1186
 1187
 1188
 1189
 1190
 1191
 1192
 1193
 1194
 1195
 1196
 1197
 1198
 1199
 1200
 1201
 1202
 1203
 1204
 1205
 1206
 1207
 1208
 1209
 1210
 1211
 1212
 1213
 1214
 1215
 1216
 1217
 1218
 1219
 1220
 1221
 1222
 1223
 1224

1225 with Percolator. For SILAC-based protein quantification, peptides XICs (Extracted
1226 Ion Chromatograms) were retrieved from Thermo Scientific Proteome Discoverer or
1227 computed with MassChroQ version 1.2.1 (51). Global MAD normalization or not was
1228 applied on the total signal to correct the XICs for each biological replicate. Protein
1229 ratios were computed as the geometrical mean of related peptides. To estimate ratio
1230 significance, a t-test was performed with the R package limma (52) and the false
1231 discovery rate has been controlled thanks to the Benjamini-Hochberg procedure (53)
1232 with a threshold set to 0.05.
1233 The mass spectrometry proteomics data have been deposited to the ProteomeX-
1234 change Consortium via the PRIDE (54) partner repository with the dataset identifier
1235 PXD012291.
1236 **Bioinformatics analysis**
1237 myProMS (v 3.5) (50) was used to analyze SILAC results. Proteins from infected
1238 secretomes were considered as differentially secreted from uninfected secretomes
1239 when showing a fold change above or less than 2, $p < 0.05$ and at least 3 detected
1240 peptides. Fold change-based gene ontology (GO) enrichment analysis was performed
1241 as in (55). SignalP 4.0 (56) was used to determine which proteins contained a signal
1242 peptide (predicted or confirmed). SecretomeP 2.0 (57) was used to detect non-
1243 conventional secretion; proteins above a cut-off of 0.5 were considered as secreted
1244 proteins. GO terms (58) were extracted from PANTHER (59) and UniprotKB.
1245 **Transferrin (Tf) recycling and endocytosis**
1246 For Tf recycling experiments, Hep2 cells cultured in 6-well plates were incubated at
1247 RT with DMEM-Hepes (UI) or the indicated bacterial strains expressing GFP or dsRed
1248 proteins at a MOI of 100. After 15 minutes of infection, human Tf coupled to Alexa
1249 Fluor 647 (Tf-AF647) (Invitrogen) was added at 0.5 $\mu\text{g}/\text{mL}$ in DMEM-Hepes-0.1% BSA
1250 at 37 °C. After 30 min of incubation to allow Tf-AF647 endocytosis, surface Tf-AF647
1251 was removed by treating cells with ice-cold sodium acetate 20 mM pH 3.0 for 3
1252 minutes at 4 °C before neutralization with DMEM-HEPES pH 10. Cells were incubated
1253 back at 37 °C in DMEM-Hepes-0.1% BSA supplemented with 50 $\mu\text{g}/\text{mL}$ of human non-
1254 fluorescent holo-transferrin to perform a time course. Cells were scraped gently and
1255 transferred into ice-cold PBS for flow cytometry (FC) analysis.
1256 For Tf endocytosis, Hep2 cells were uninfected or infected with GFP-expressing
1257 relevant strains as previously described. After 60 min of infection at MOI 10, cells
1258 were washed twice with warm DMEM-Hepes and incubated for additional 30 min in
1259 the same medium containing 0.1% BSA and gentamicin 50 $\mu\text{g}/\text{mL}$ to kill extracellular
1260 bacteria. Tf uptake time-course was performed by incubating cells in a water
1261 bath at 37 °C with DMEM-Hepes-0.1% BSA in the presence of 0.5 $\mu\text{g}/\text{mL}$ Tf-AF647
1262 for different time points, followed by an acid stripping of remaining membrane
1263 associated Tf-AF647.
1264 To measure surface TFR levels, UI or infected cells were incubated at 4 °C in the
1265 presence of Tf-AF647 for 30 minutes. Cells were acid washed or untreated, and the
1266 total surface Tf-AF647 fluorescence was quantified by FC.
1267 Where indicated, cells were transfected with the relevant plasmids the day before
1268 the Tf recycling or endocytosis experiments by electroporation (10 μg DNA/4.5x10⁶
1269 cells) or using Lipofectamine 3000 (Thermo Fischer Scientific).
1270 The Geometrical Mean Fluorescence of intracellular Tf-AF647 was measured in gated
1271 living cells (using Dapi or Live/Dead Fixable Violet Cell Stain Kit, L34955, Molecular
1272 Probes) by FC in a BD FACSCanto II Flow Cytometer (BD Biosciences) or an Attune
1273 NxT Flow Cytometer (Thermo Fischer Scientific). Tf recycling results were expressed
1274 as the percentage of the remaining intracellular Tf-AF647 at each time point respect
1275 to time 0 of recycling. Tf recycling rate was determined from the slope of ln2 data
1276 during the first 30 minutes of kinetics. Tf endocytosis results were expressed as Tf
1277 endocytosis rate, calculated as the internal Tf-AF647 fluorescence over time, during
1278 the first 10 minutes of kinetics.
1279 **IL-2R β endocytosis**
1280 Hep2 β cells seeded on 12-mm coverslips were uninfected or infected with GFP-
1281 expressing bacteria. After 90 min of infection, a time-course of IL-2R β endocytosis
1282 was performed by incubating cells with an anti-IL-2R β antibody (mouse Ab 561)
1283 conjugated to Cy3 (1:1000) (44) at 37 °C for different time points. Cells were fixed,
1284 permeabilized and stained with HCS CellMask Blue Stain (Molecular Probes) and
1285 Phalloidin-AF647 or Tf-AF647. Imaging was performed by TIRF microscopy. IL-2R β
1286 endocytosis was quantified with ICY software as described in (21).
1287 **Animals, infections and sample preparation**
1288 Guinea pigs were infected according to previously described protocols (27, 28).
1289 Female specific pathogen-free Hartley guinea pigs (120–250 g) were purchased from
1290 Charles River Laboratories, maintained in animal care facilities of Institut Pasteur,
1291 and provided with food and water *ad libitum*. Animal experiments were carried out
1292 under approval by the "Use Committee of Institut Pasteur and by the French Ministry
1293 of Agriculture no. 2013-0113". Briefly, animals were anesthetized intraperitoneally
1294 using a mixture of ketamine (100 mg/kg; Merial) and xylazine hydrochloride (10
1295 mg/kg; Bayer) before intrarectal inoculation of *S. flexneri* strains at 5x10¹⁰ cfu per
1296 200 μL . Animals were sacrificed at 4 and 8 hours postchallenge. The distal 10 cm of
1297 colon was harvested and fixed overnight in 4% (vol/vol) PFA in PBS, and incubated
1298 in PBS-glycine (100 mM) for 30 min to quench the PFA. Tissues were then immersed
1299 successively in 15% and 30% (wt/vol) sucrose at 4 °C overnight. Tissues were cut and
1300 embedded in Tissue-Tek OCT compound (Sakura) using a flash-freeze protocol and
1301 frozen at -80 °C.

1302 **Immunofluorescence**
1303 Hep2 and Hep2 β cells were fixed in PFA 4% sucrose 4% in PBS for 20 min and
1304 quenched with NH₄Cl 50 mM for 10 min. Permeabilization, blocking, incubations
1305 and washes were done with PBS BSA 0.1% saponin 0.05%. Polarized Caco-2/Tc7 cells
1306 were washed, fixed and quenched preparing solutions in PBS with Ca²⁺ and Mg²⁺
1307 (Gibco). Permeabilization was done in PBS Ca²⁺ Mg²⁺ gelatin 0.2%, saponin 0.075%
1308 for 1 hour at RT, primary antibodies incubated for 90 min at RT or overnight at 4
1309 °C, secondary antibodies 1 hour at RT, together with Dapi 1 $\mu\text{g}/\text{mL}$ and Phalloidin
1310 coupled to AlexaFluor (Molecular Probes) if indicated.
1311 For tissue sections, immunofluorescence samples were prepared as follows: 10 μm -
1312 thick transversal colon sections were permeabilized in PBS 0.5% Triton X-100 for 30
1313 min, blocked in PBS 1% BSA for 30 min at RT and incubated overnight at 4 °C with the
1314 indicated primary antibodies, together with Phalloidin AlexaFluor 647 (1:100) diluted
1315 in PBS, 0.1% Triton X-100, 1% BSA. Sections were then washed with PBS and stained
1316 for 1–2 hours at RT with AlexaFluor 568 goat anti-mouse or anti-rabbit (A11031 and
1317 A11036; Molecular Probes), followed by incubation with Dapi (1 $\mu\text{g}/\text{mL}$) for 10 min
1318 at RT. Samples were washed with PBS before mounting.
1319 ProLong Gold Antifade (Molecular Probes) was used as mounting medium.
1320 **Image acquisition**
1321 The following equipment was used for image acquisition: a LSM700 inverted laser
1322 scanning confocal microscope (Zeiss), with a 40x/1.4 Oil immersion or a 63x/1.4 Oil
1323 immersion objective (Zeiss); an Axio Observer.Z1 microscope (Zeiss) equipped with a
1324 swept field confocal Opterra system (Bruker) and an Evolve 512 Delta EMCCD camera
1325 (Photometrics), using a 63x PlanAPO-CHROMAT oil immersion/1.4 NA objective
1326 (Zeiss); a slide scanner Axio Scan.Z1 (Zeiss), using a 40x dry objective; an inverted
1327 confocal microscope LSM 780 Elyra PS.1 (Zeiss), using an alpha Plan Apo 100X/1.46
1328 NA oil objective (Zeiss) (TIRF imaging).
1329 **Image analysis and quantification**
1330 Microscopy images were processed and quantified with Fiji (ImageJ) (60), ICY soft-
1331 ware (61) (<http://icy.bioimageanalysis.org>) or Zen (Zeiss). Colocalization quantifica-
1332 tion was performed on confocal images using the Statistical Object Distance Analysis
1333 (SODA) plugin in ICY software described in (62). IL-2R β endocytosis was quantified
1334 with ICY software using "HK-Means" and "Active Contours" plugins to automatically
1335 detect cell boundaries and "Spot Detector" plugin to measure the number of the IL-
1336 2R β spots within the detected cells. The total intensity of IL-2R β spots was normalized
1337 to the mean value of the uninfected conditions. Quantification of Dnm2 or CLC
1338 density at plasma membrane from TIRF images was performed using ICY "Spot
1339 detector" plugin to quantify the number of spot per cell area. Quantification of Tf-
1340 A647 uptake by Caco-2/Tc7 cells was performed with Fiji, by quantifying the total
1341 fluorescence per cell from 10 slices of 0.8 μm from a z-stack. Tissue images were
1342 acquired with 40X objectives and subsequent stitching was performed using Zen
1343 software to build the mosaic images. Quantification of bacteria depth penetration
1344 into the intestinal mucosa was done from images illustrated in Fig. S4C with Fiji,
1345 by measuring the maximum bacterial distance of penetration from the epithelium
1346 surface, respect to the total mucosal thickness.
1347 **Data presentation and statistical analysis**
1348 Prism 6.0 (GraphPad Software, Inc.) was used to perform statistical analysis. Results
1349 are represented as mean \pm SD, except otherwise indicated. The following statistical
1350 tests were used: Welch's t-test performed as unpaired two-tailed analysis; one-way
1351 ANOVA followed by Dunnett's or Tukey's *post-hoc* multiple comparison tests; Mann-
1352 Whitney; Kruskal-Wallis followed by Dunn's *post-hoc* test. $P < 0.05$ was considered
1353 significant for all analyses.
1354 Fiji and Zen (Zeiss) were used to process microscopy images. Inkscape software
1355 (<http://www.inkscape.org/>) was used for assembling figures.